Original Article

Institution of MECHANICAL ENGINEERS
Journal of AEROSPACE ENGINEERING

Proc IMechE Part G:
J Aerospace Engineering
0(0) 1–16

DOI: 10.1177/0954410018785971
journals.sagepub.com/home/pig
SAGE

Fast solution of minimum-time low-thrust transfer with eclipses

Max Cerf

Abstract

Optimizing low-thrust orbital transfers with eclipses by indirect methods raises several issues, namely the costate discontinuities at the eclipse entrance and exit, the initial costate guess sensitivity and the numerical accuracy required by the shooting method. The discontinuity issue is overcome by detecting the eclipse within the simulation and applying the costate jump derived analytically from the shadow constraint function. By fixing completely the targeted final position and velocity, the transversality conditions are removed and the shooting problem is recast as an unconstrained nonlinear programming problem. The numerical sensitivity issues are alleviated by using a derivative-free algorithm. The search space is reduced to four angles taking near zero values. This procedure yields a quasi-optimal solution from scratch in few minutes without requiring any specific user's guess or tuning. The method is applicable whatever the thrust level and the eclipse configuration, as illustrated on transfers towards the geostationary orbit.

Keywords

Orbital transfer, low-thrust, eclipse, costate guess, optimal control

Date received: 11 July 2017; accepted: 4 June 2018

Introduction

Electric rocket engines offer promising propellant savings for orbital transfers at the expense of long durations due to very low-thrust levels. Minimum-time low-thrust trajectories are consequently studied intensively for several decades. An additional difficulty comes from the large power required by electric propulsion engines, impeding their use during the transit in the Earth shadow. The minimum-time low-thrust transfer between two orbits formulates as an optimal control problem (OCP) with dynamics discontinuities at the eclipse entrances and exits.

Various approaches have been applied to solve such OCP s as efficiently as possible. They are classified between direct and indirect methods.[1–3]

Direct methods discretize the OCP in order to rewrite it as a nonlinear large-scale optimization problem. Various discretization methods can be chosen for the dynamics and for the control.[4–9] This process is straightforward and new variables or constraints may be added to the problem with reduced programming effort. Several software packages, such as IPOPT, BOCOP, GESOP, SNOPT, WORHP, etc., are available to solve the large-scale optimization problem. The direct approach is suitable to a wide range of applications. The main drawback is that it is computationally expensive when the number of variables becomes large, which is especially the case for low-thrust transfers.[10–13] Finding an accurate solution for such problems may be difficult. An alternate discretization approach which reduces the problem size consists in approximating the dynamics by a series of impulsive maneuvers.[13–16]

On the other hand, indirect methods are based on the Pontryagin maximum principle (PMP)[17,18] which gives a set of necessary conditions for a local optimal solution. For minimum-time problems the PMP yields the optimal thrust direction aligned with the velocity costate.[19–22] The problem is reduced to a two-point boundary value problem (BVP). The resulting nonlinear system is generally solved by a shooting method using a Newton-like algorithm. The convergence is fast and accurate, but the method requires both an adequate starting point and a high integration accuracy. These are major issues when applying the indirect approach to low-thrust transfers,[23,24] particularly in the case of dynamics discontinuities.[25] Moreover, the problem may admit singular solutions for which the PMP first-order conditions no longer define the optimal control. Such singular solutions

Ariane Group, Les Mureaux, France

Corresponding author:
Max Cerf, Ariane Group, 78130 Les Mureaux, France.
Email: max.cerf@numericable.fr

require further theoretical analysis and specific solution methods.[26,27]

For low-thrust transfers, various approaches can be envisioned to build a satisfying initial costate guess and benefit from the efficiency of the indirect method. In Augros et al.,[28] the impulse transfer solution is used to provide a good initial guess to the shooting algorithm. This method is based on the fact that a continuous high-thrust orbit transfer exhibits similarities with the impulse transfer as outlined in Naidu et al.[29] and Gergaud and Haberkorn.[30] Analytical costate approximation are derived in Lee and Bang[31] for transfers between circular orbits. In Pifko et al.,[32] the similarity between the double integrator and the orbital transfer is exploited to propose an analytical costate guess. Multiple shooting reduces the overall sensitivity by splitting the trajectory in several arcs at the expense of additional unknowns and boundary conditions. In Oberle and Taubert,[33] a multiple shooting method parameterized by the number of thrust arcs is used to solve an Earth–Mars transfer. The multiple shooting is combined with a collocation method in Graham and Rao[34] by splitting the trajectory into thrust and coast arcs in the Earth shadow. Homotopic approaches[35] solve a series of optimization problems by continuous transformation starting from a known solution. In Bonnard et al.[23] and Gergaud et al.,[36] a differential continuation method linking the minimization of the L^2-norm of the control to the minimization of the consumption is used to solve the low-thrust orbit transfer around the Earth. In Haberkorn and Trélat,[37] a regularization procedure is applied to smoothen the costate discontinuities the coplanar low-transfer problem with eclipses is solved by a continuation on the regularization parameter. Convergence results are established showing that the original problem solution is recovered. In Thorne and Hall,[38] simplified formulas are established by interpolating many numerical experiments, which allows a successful initialization for the minimal time orbit transfer problem, in a given range of nearly circular initial and final orbits. Based on that initial guess and averaging techniques, the software T3D[39] implements continuation and smoothing processes in order to solve minimal time or minimal fuel consumption orbit transfer problems. Particle swarm,[40] genetic algorithms,[41] or other metaheuristics[42] can also be used to explore largely the variables space and produce a satisfying initial solution. One can also mention mixed methods that use a discretization of the PMP necessary conditions and then apply a large-scale equation solver[43] and dynamic programming methods that search for the global optimum in a discretized state space by solving the Hamilton–Jacobi–Bellman equation.[44] In order to account for eclipsing on low-thrust transfers various solution methods have been investigated: semi-analytical solutions for near circular orbits by Kechichian,[45–47] direct approaches,[12,34,48–50] indirect approaches,[37,51] Lyapunov feedback control (or Q-law) developed by Petropoulos.[52–54]

This paper deals with the minimum-time orbital transfer with eclipses solved by an indirect approach. A solution method is proposed that avoids the issues linked to the costate discontinuities at the eclipse bounds, to the initial costate guess and to the overall numerical sensitivity of the shooting method. The dynamical model with eclipses is presented in §2.1. The OCP is formulated in §2.2 and the costate discontinuities are derived from the optimality conditions. The boundary value problem is recast in §2.3 as an unconstrained minimization problem with only four unknowns. An analytical costate guess is defined that reduces the search space to narrow intervals around zero and the unconstrained minimization problem is solved by a derivative-free algorithm. By this way, an accurate numerical propagation is no longer mandatory as is the case with Newton-like methods. Rectangular coordinates can be used (making the dynamics equations and the eclipse conditions simple) with large time steps and less stringent tolerance on the numerical integration error. A typical application case is presented in §3 for various initial dates, orbit orientations, and engine thrust levels.

Problem formulation and solution method

This section formulates the OCP for a minimum-time low-thrust orbital transfer accounting for eclipses. The costate discontinuities at the eclipse entrance and exit are derived from the optimality conditions. The boundary value problem is then recast as a small size unconstrained minimization problem.

Dynamical model

The problem consists in finding the minimum-time trajectory to transfer a low-thrust vehicle from an initial orbit to a final orbit. The Earth is modeled as a sphere, with a central gravity field. The vehicle is modeled as a material weighting point with position $\vec{r}(t)$, velocity $\vec{v}(t)$, and mass $m(t)$. It is submitted to the Earth acceleration gravity denoted $\vec{g}(\vec{r})$ and to the engine thrust denoted $\vec{T}(t)$. The thrust direction can be chosen freely, and it is directed along the unit vector $\vec{u}(t)$. The thrust level T is constant with a burned propellant exhaust velocity equal to v_e. The mass flow-rate is the ratio of the thrust to the exhaust velocity. During eclipses the engine has to be switched off to spare the on-board power. The dynamical model must therefore account for the Sun relative motion with respect to the Earth in order to determine the eclipse phases along the vehicle trajectory. Only the Sun direction is used to determine the Earth shadow region. Neither the solar attraction nor the radiation pressure is considered in the dynamics.

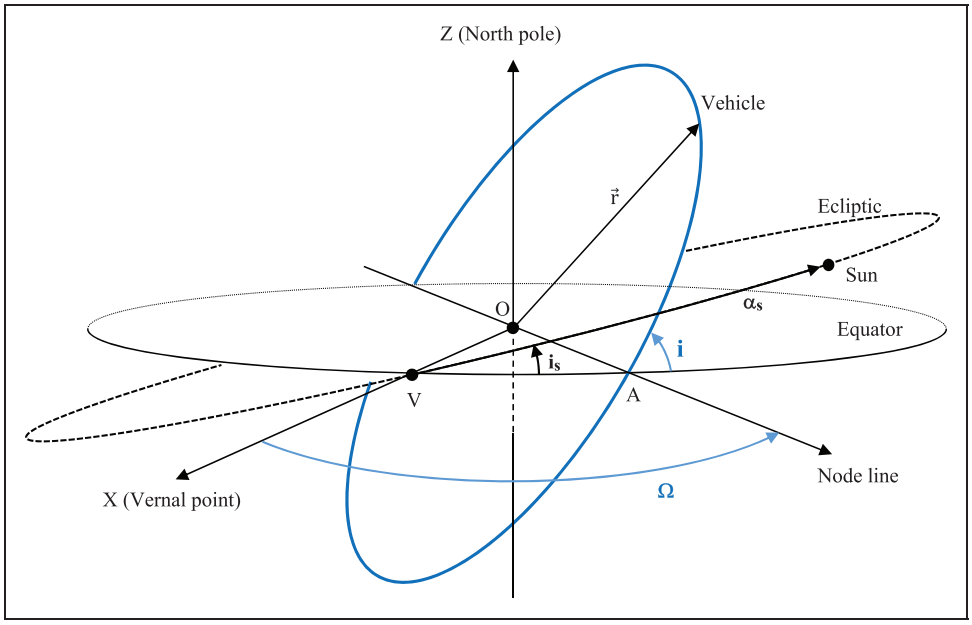

Figure 1. Sun and vehicle motion in ECI frame.

The motion equations are written in an Earth-centered inertial (ECI) reference frame (O, X, Y, Z) with the origin O at the Earth center, the X and Z axes pointing respectively toward the vernal point and the North pole, and the Y axis completing the frame. The relative motion of the Sun with respect to the Earth occurs in the ecliptic plane. This plane is 23.45° inclined on the equatorial plane (equatorial obliquity denoted i_s), with an intersection along the X axis as depicted on Figure 1. The Sun anomaly α_s is measured from the X axis. The initial anomaly α_0 at the date $t_0 = 0$ depends on the transfer starting day. The values $\alpha_0 = 0°$, 90°, 180°, and 270° correspond respectively to the spring equinox, the summer solstice, the autumn equinox, and the winter solstice. The anomaly α_s evolves linearly with the time, at the angular rate $\omega_s = 360°/\text{year}$. The Sun direction in the ECI frame is given by

$$\vec{e}_s = \begin{pmatrix} \cos\alpha_s \\ \sin\alpha_s \cos i_s \\ \sin\alpha_s \sin i_s \end{pmatrix} \quad \text{with} \quad \begin{cases} \alpha_s(t) = \alpha_0 + \omega_s t \\ i_s = 23.45° \\ \omega_s = 0.986°/\text{day} \end{cases} \tag{1}$$

The eclipse conditions depend on the vehicle position $\vec{r}(t)$ and the Sun direction $\vec{e}_s(t)$ as depicted on Figure 2. The Earth shadow is assumed to be a cylinder having the radius of the Earth R_E. An alternative model is a conic shape centered at the Sun. The difference between these models is not significant for a low-thrust transfer.

An eclipse occurs when the following conditions are met ($^\Lambda$ denotes the cross-product operator).

$$\begin{cases} \left\| \vec{e}_s \Lambda \vec{r} \right\| < R_E \\ \vec{e}_s . \vec{r} < 0 \end{cases} \tag{2}$$

The first condition expresses that the vehicle is inside the shadow cylinder, the second condition checks that the vehicle and the Sun stand in opposite directions with respect to the Earth. The shadow function ψ_s is defined as

$$\psi_s(\vec{r}, t) = \left\| \vec{e}_s \Lambda \vec{r} \right\|^2 - R_E^2 \tag{3}$$

This function changes sign at the eclipse entrance and exit. When the vehicle enters the Earth shadow, the engine is switched off. Applying the fundamental dynamics principle in the ECI frame yields the motion equations respectively in the light and shadow regions. The dependencies on time (for $\vec{r}$, $\vec{v}$, m, and $\vec{u}$) are omitted for conciseness.

$$\begin{cases} \dot{\vec{r}} = \vec{v} \\ \dot{\vec{v}} = \vec{g}(\vec{r}) + \frac{\varepsilon T}{m} \vec{u} \quad \text{with} \quad \varepsilon = 1 \text{ in light} \\ \dot{m} = -\frac{\varepsilon T}{v_e} \qquad\qquad\quad \varepsilon = 0 \text{ in shadow} \end{cases} \tag{4}$$

The variable ε is equal to 0 (respectively 1) inside (respectively outside) the shadow region.

A dynamics discontinuity occurs whenever entering or leaving the shadow region, corresponding to a zero of the function ψ_s. This condition acts as an interior point constraint for the OCP.

Optimal control problem

The OCP is formulated considering as state variables $\vec{r}(t)$, $\vec{v}(t)$, m(t) and as control variables the thrust direction $\vec{u}(t)$ and the final time t_f. The initial state and the final orbit are prescribed. The vehicle location on the final orbit is defined by the anomaly. For a low-thrust transfer with many revolutions, the final anomaly has a negligible influence on the solution and it

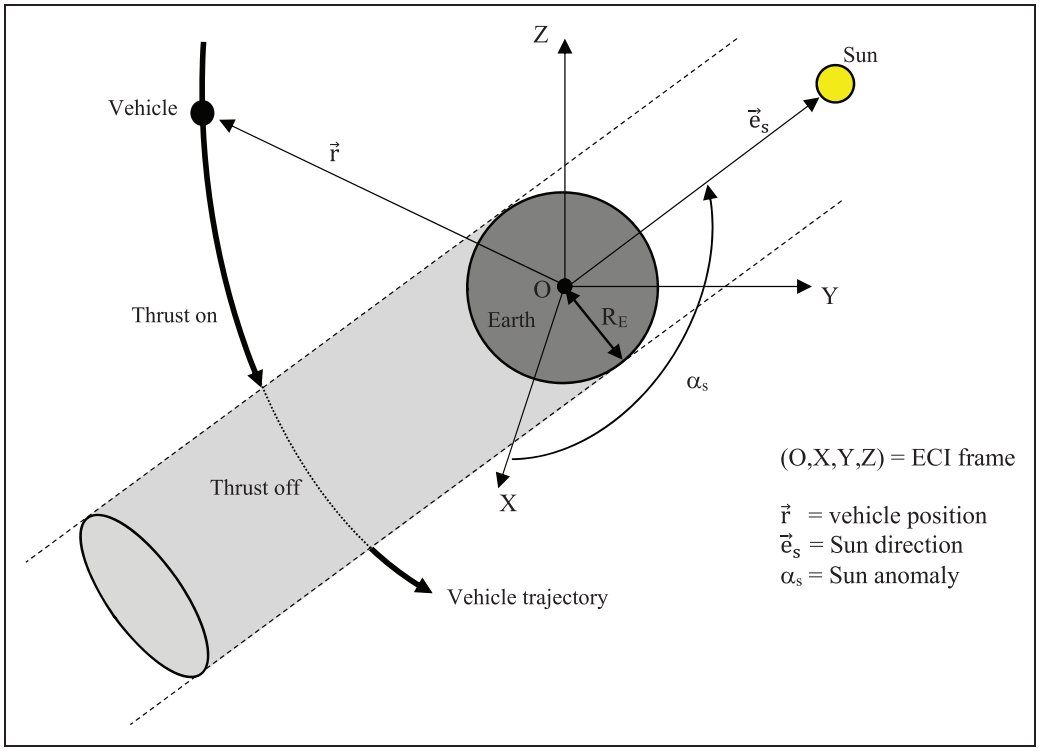

Figure 2. Eclipse conditions. ECI: Earth-centered inertial.

can be constrained to zero, i.e., at the targeted orbit perigee. The final position and velocity become thus completely prescribed and the corresponding transversality conditions are removed, which simplifies the solution procedure.

For a minimum-time transfer, the OCP formulation is

$$\min_{\vec{u}(t),\,t_f} J = t_f \text{ s.t.} \begin{cases} \dot{\vec{r}} = \vec{v} \\ \dot{\vec{v}} = \vec{g} + \frac{\varepsilon T}{m}\vec{u} \\ \dot{m} = -\frac{\varepsilon T}{v_e} \end{cases} \text{with} \begin{cases} \vec{r}(t_0) = \vec{r}_0 \\ \vec{v}(t_0) = \vec{v}_0 \\ m(t_0) = m_0 \end{cases} \text{fixed initial state} \quad \begin{cases} \vec{r}(t_f) = \vec{r}_f \\ \vec{v}(t_f) = \vec{v}_f \end{cases} \text{constrained final state} \tag{5}$$

The dynamics are discontinuous at the eclipse entrance and exit. The number of such discontinuities is unknown a priori since it depends on the number of revolutions performed during the transfer. The problem is not autonomous because it depends on the initial date t_0 which defines the Sun anomaly α_0, and on the initial orbit orientation in the ECI frame.

The optimal trajectory is sought by applying PMP.[17,18] For that purpose, the costate vectors $\vec{p}_r(t)$, $\vec{p}_v(t)$, and $p_m(t)$ are introduced associated respectively to the position, the velocity, and the mass. These costate vectors do not vanish identically on any interval of $[t_0, t_f]$ and they are defined up to a non-positive scalar multiplier p_0. The usual normalization for regular extremals is chosen with $p_0 = -1$.

With these notations, the Hamiltonian for the OCP equation (5) is

$$\begin{aligned} H &= \vec{p}_r.\dot{\vec{r}} + \vec{p}_v.\dot{\vec{v}} + p_m\dot{m} = \vec{p}_r.\vec{v} + \vec{p}_v.\left(\vec{g} + \frac{\varepsilon T}{m}\vec{u}\right) + p_m\left(-\frac{\varepsilon T}{v_e}\right) \\ &= \vec{p}_r.\vec{v} + \vec{p}_v.\vec{g} + \varepsilon T\left(\frac{\vec{p}_v.\vec{u}}{m} - \frac{p_m}{v_e}\right) \end{aligned} \tag{6}$$

The PMP provides first-order necessary conditions that must be satisfied by an optimal trajectory.

- The Hamiltonian maximization condition with respect to the control $\vec{u}(t)$ yields the thrust direction aligned with the velocity costate

$$\max_{\vec{u}} H \Rightarrow \vec{u} = \frac{\vec{p}_v}{p_v} \text{ with } p_v = \left\|\vec{p}_v\right\| \tag{7}$$

The Hamiltonian equation (6) becomes

$$H = \vec{p}_r.\vec{v} + \vec{p}_v.\vec{g} + \varepsilon T\Phi \quad \text{with } \Phi = \frac{p_v}{m} - \frac{p_m}{v_e} \tag{8}$$

- The costates follow differential equations with transversality conditions at the final date. The final position and velocity costates are free since the final position and velocity are completely prescribed. The final mass costate is derived from the final cost t_f.

$$\begin{cases} \dot{\vec{p}}_r = -\frac{\partial H}{\partial \vec{r}} = -\frac{\partial \vec{g}}{\partial \vec{r}}\vec{p}_v, & \vec{p}_r(t_f) = \text{free} \\ \dot{\vec{p}}_v = -\frac{\partial H}{\partial \vec{v}} = -\vec{p}_r, & \vec{p}_v(t_f) = \text{free} \cdot \\ \dot{p}_m = -\frac{\partial H}{\partial m} = \frac{\varepsilon T}{m^2} p_v, & p_m(t_f) = 1 \end{cases} \tag{9}$$

- The free final time t_f satisfies the transversality condition

$$H(t_f) = -1 \tag{10}$$

The dynamics discontinuity at the shadow entrance or exit generates discontinuities on the costate components and on the Hamiltonian.[55,56] A discontinuity occurs whenever the shadow function ψ_s vanishes with the vehicle and the Sun standing in opposite directions. Each date t_d of eclipse entrance or exit satisfies the following interior point constraint.

$$\psi_s\left[\vec{r}(t_d), t_d\right] = \left\|\vec{e}_s(t_d) \Lambda \vec{r}(t_d)\right\|^2 - R_E^2 = 0 \tag{11}$$

The costate and Hamiltonian discontinuities at t_d are given by

$$\begin{cases} \Delta\vec{p}_r(t_d) = -\nu \frac{\partial \psi_s}{\partial \vec{r}} \\ \Delta\vec{p}_v(t_d) = -\nu \frac{\partial \psi_s}{\partial \vec{v}} \Rightarrow \Delta\vec{p}_v(t_d) = \vec{0} \\ \Delta p_m(t_d) = -\nu \frac{\partial \psi_s}{\partial m} \Rightarrow \Delta p_m(t_d) = 0 \\ \Delta H(t_d) = \nu \frac{\partial \psi_s}{\partial t} \end{cases} \tag{12}$$

where ν is an unknown multiplier associated to the interior point constraint.

To find the multiplier value, the Hamiltonian equation (8) is written just before and just after the discontinuity date. The state is continuous. The only discontinuous variables are the position costate $\vec{p}_r$ from equation (12) and the coefficient ε which switches from 1 to 0 (eclipse entrance) or from 0 to 1 (eclipse exit).

$$\begin{cases} H\left(t_d^-\right) = \vec{p}_r\left(t_d^-\right).\vec{v} + \vec{p}_v.\vec{g} + \varepsilon\left(t_d^-\right)T \\ H\left(t_d^+\right) = \vec{p}_r\left(t_d^+\right).\vec{v} + \vec{p}_v.\vec{g} + \varepsilon\left(t_d^+\right)T \end{cases} \tag{13}$$

Subtracting both equations yields a relationship between the Hamiltonian and the costate discontinuity.

$$\Delta H(t_d) = \Delta\vec{p}_r(t_d).\vec{v} + \Delta\varepsilon(t_d)T\Phi \tag{14}$$

Using equation (12) to replace ΔH and $\Delta\vec{p}_r$, an explicit expression is obtained for the multiplier ν.

$$\nu = \frac{T\Phi\Delta\varepsilon}{\dot{\psi}_s} \text{ with } \dot{\psi}_s = \frac{\partial \psi_s}{\partial t} + \frac{\partial \psi_s}{\partial \vec{r}}.\vec{v} \tag{15}$$

where $\dot{\psi}_s$ is the total derivative of the shadow function ψ_S along the vehicle trajectory and $\Delta\varepsilon = -1$ (respectively $+1$) at the shadow entrance (respectively exit).

The total derivative $\dot{\psi}_s$ is computed from equation (11) by applying the cross and dot product derivation rules.

$$\dot{\psi}_s = \frac{d}{dt}\left\|\vec{e}_s \Lambda \vec{r}\right\|^2 = 2\left(\vec{e}_s \Lambda \vec{r}\right).\left(\dot{\vec{e}}_s \Lambda \overrightarrow{r} + \vec{e}_s \Lambda \vec{v}\right) \tag{16}$$

In this expression, $\vec{r}$ and $\vec{v}$ are the vehicle position and velocity at the date t_d, and $\vec{e}_s$ is the Sun direction at t_d whose derivative is obtained from equation (1).

$$\dot{\vec{e}}_s = \omega_s \begin{pmatrix} -\sin\alpha_s \\ \cos\alpha_s \cos i_s \\ \cos\alpha_s \sin i_s \end{pmatrix} \tag{17}$$

With the equations (15) to (17), the costate discontinuities equation (12) can be assessed and applied directly within the propagation of the state and costate equations, provided that the dates of shadow entrance and exit are properly detected within the numerical integration. The optimal trajectory is then solution of the following BVP.

Boundary value problem. Find the initial costates $\vec{p}_r(t_0)$, $\vec{p}_v(t_0)$, $p_m(t_0)$, and the final time t_f such that the final state constraints equation (5), and the transversality conditions equations (9) and (10) on $p_m(t_f)$ and $H(t_f)$ are met.

The shooting method consists in solving this nonlinear system of dimension eight by a Newton-like method with a numerical integration of the state and costate differential equations from the initial date to the final date. A major issue of this approach lies in the high sensitivity to the initial costate guess. Without a careful initialization, an accurate numerical integration,[25] and regularization procedures,[37] the Newton method is very likely to fail. This behavior is especially marked for low-thrust transfers which need very long propagation durations (several days or weeks or even months) and dynamics discontinuities (due to eclipses). Finding a satisfying costate guess for such low-thrust transfers is a major challenge which may discourage from applying the shooting method.

Solution method

The solution method proposed aims at avoiding the shooting method issues, due to the costate guess and

to the numerical accuracy required by the Newton method.

The first part of the solution method consists in defining an accurate costate guess. For that purpose, some past results about orbital transfers are used.

A first useful result is that for minimum-time low-thrust transfers the propellant consumption and the total velocity impulse are nearly insensitive to the thrust level.[30,57–59] When the transfer time becomes large, the following relationship is observed.

$$m_0 - m_f = \frac{T t_f}{v_e} \approx C^{te}, \quad \forall T \tag{18}$$

A second useful result is that for minimum-fuel high-thrust coplanar transfers at constant optimized thrust level, there exists an analytical costate solution, with orthogonal position and velocity costates.[60]

$$\vec{p}_r(t_0) = \omega_0 \begin{pmatrix} -\cos\theta_0 \\ \sin\theta_0 \end{pmatrix}, \vec{p}_v(t_0) = \begin{pmatrix} \sin\theta_0 \\ \cos\theta_0 \end{pmatrix},$$
$$p_m(t_0) = \frac{v_e}{m_0} \tag{19}$$

In these formulae, θ_0 is the initial pitch angle (angle between the horizontal and the thrust direction). It depends on the initial conditions (radius vector r_0, velocity modulus v_0, and flight path angle γ_0) through the implicit equation

$$\sin(\theta_0 - \gamma_0) = \frac{v_{c0}}{v_0} \frac{\sin\theta_0}{\sqrt{1 - 3\sin^2\theta_0}} \text{ with } v_{c0} = \sqrt{\frac{\mu}{r_0}} \tag{20}$$

where ω_0 is the thrust initial rotation rate given by

$$\omega_0 = \sqrt{\frac{\mu}{r_0^3}(1 - 3\sin^2\theta_0)} \tag{21}$$

The final mass for a low-thrust transfer being nearly insensitive to the thrust level, it can be hoped that the above formulae can be successfully reused as costate guess for low-thrust transfers. Nevertheless the equations (19) to (21) apply only to coplanar transfers. For a plane change, an out-of-plane component must be introduced in the initial costate guess. This leads to the following guess parameterized by two in-plane angles θ_r and θ_v, and two out-of-plane angles β_r and β_v. The in-plane angle θ is the angle between the vector projected in the local orbital plane and the initial velocity (which is horizontal since the transfer starts at the perigee). The out-of-plane angle β is the angle between the vector and the local orbital plane.

$$\vec{p}_r(t_0) = \omega_v \begin{pmatrix} -\cos\theta_r \cos\beta_r \\ \sin\theta_r \cos\beta_r \\ \sin\beta_r \end{pmatrix},$$
$$\vec{p}_v(t_0) = \begin{pmatrix} \sin\theta_v \cos\beta_v \\ \cos\theta_v \cos\beta_v \\ \sin\beta_v \end{pmatrix}, \quad p_m(t_0) = \frac{v_e}{m_0} \tag{22}$$

$$\text{with } \omega_v = \sqrt{\frac{\mu}{r_0^3}(1 - 3\sin^2\theta_v)} \tag{23}$$

For a low-thrust transfer starting at the perigee, it is expected that these four angles take small values. This corresponds to a thrust nearly aligned with the initial velocity and a nearly null out-of-plane component at the transfer beginning. With that guess the search space can be reduced to a narrow interval of a few degrees around zero for all angles. The mass costate does not need any specific guess since it does not influence the evolution of the position and velocity costates equation (9) which define completely the control $\vec{u}$ by equation (7). The four angles θ_r, θ_v, β_r, and β_v define therefore the complete command law along the trajectory.

The second part of the solution method consists in reducing the BVP to an unconstrained minimization problem. In most practical cases, the transfer aims at raising the vehicle up to a high-altitude orbit such as the geostationary orbit (GEO). For such transfers, the perigee altitude is monotonously increasing along the trajectory, and the transfer is achieved as soon as the perigee reaches the targeted altitude. This property can be exploited to discard the final date from the problem unknowns. The numerical integration is stopped when the perigee reaches the desired value. The problem reduces to finding the four angles values θ_r, θ_v, β_r, and β_v in order to reach the targeted final position $\vec{r}_f$ and velocity $\vec{v}_f$. This problem is recast as an unconstrained nonlinear programming problem.

$$\min_{\theta_r, \theta_v, \beta_r, \beta_v} \frac{\left\|\vec{r}(t_f) - \vec{r}_f\right\|}{\left\|\vec{r}_f\right\|} + \frac{\left\|\vec{v}(t_f) - \vec{v}_f\right\|}{\left\|\vec{v}_f\right\|} \tag{24}$$

The cost function sums the normalized differences between the actual and targeted final position and velocity. This cost function must be brought close to zero. It is not mathematically guaranteed that this formulation actually yields the minimum-time trajectory. Different sets of values (θ_r, θ_v, β_r, and β_v) could indeed exist that allow reaching the targeted orbit with different final times. In practice, the interval of search for these angles (with an initial thrust direction making a small angle with the velocity) is very narrow so that the trajectory obtained should be close to optimal. This has been checked on the application cases presented in §3, by comparing to existing literature results.

The third part of the solution method consists in the minimization algorithm choice. The propagation of the state and costate differential equations on long durations is prone to numerical errors. The inaccuracy is increased by the numerous discontinuities due to eclipses. The transitions at the shadow region bounds must be very accurately detected to ensure the smoothness of the integration result. These numerical errors may have very adverse effects for gradient-based optimization algorithms.[61] Derivative-free optimization

methods are more efficient on such "noisy" optimization problems suffering from numerical inaccuracy or poor smoothness, although they are generally less suited to constraint handling.[62,63]

The unconstrained formulation equation (24) is suited to any derivative-free optimization method.[64] A particularly attractive algorithm for this small size problem is DIRECT.[65–67] DIRECT explores the search space in a deterministic way and ensures finding the global minimum under reasonable regularity assumptions (Lipschitzian cost function). Opposite to metaheuristics like genetic algorithm, particle swarm, simulated annealing, etc. that involve a stochastic part and therefore a risk of missing the global minimum, DIRECT is able to locate correctly the solution with a controlled number of function evaluations.

With a derivative-free algorithm, it is not necessary to pay a special care on the numerical integration accuracy. For the present application, the state and costate are expressed in Cartesian coordinates. This choice is not numerically the best for a low-thrust orbital transfer, but it yields very simple equations for the state equation (4), the costate equation (9), and the eclipse constraint formulation equation (11). The eighth-order Runge–Kutta method DOP853 is used for the propagation with large time steps and large tolerances on the integration error. The eclipses are detected within the propagation and the time step is adapted by dichotomy to pass accurately at the eclipse transition date and apply the explicit costate discontinuity given by equation (12). These tunings make each simulation quite fast. The convergence of DIRECT requires about a thousand simulations and it is achieved in a few minutes in the longest cases (transfer durations of several months).

Application

The solution method is illustrated on a minimum-time low-thrust transfer from a geostationary transfer orbit (GTO) to the GEO. The Earth equatorial radius is $R_E = 6{,}378{,}137$ m and the gravitational constant is $\mu = 3.986005.10^{14}$ m^3/s^2. The initial GTO orbit has an apogee altitude of 36,000 km, a perigee altitude of 500 km, an inclination of 10°, and a perigee argument of 0° so that the apsis line lies in the Equatorial plane. The targeted GEO orbit is equatorial circular at 36,000 km. The vehicle initial gross mass is 1000 kg, and the engine thrust level is 1 N with a specific impulse of 1500 s corresponding to an exhaust velocity of 14,710 m/s.

The minimum-time transfer is computed for different initial dates and different initial orbit orientations. The initial date defines the Sun initial anomaly α_0. The initial orbit orientation (right ascension Ω of the ascending node denoted A in Figure 1) defines the perigee local time.

The derivative-free algorithm DIRECT is used to find the four angles (θ_r, θ_v, β_r, and β_v) defining the initial costate. The search intervals are respectively $[-10°$ and $+10°]$ for the in-plane angles (θ_r and θ_v) and $[-1°$ and $+1°]$ for the out-of-plane angles (β_r and β_v). With a time step of 1000 s and an accuracy of 10 s for the eclipse detection, each simulation takes on average 0.1 s on a standard Linux computer using the dynamics equations in Cartesian coordinates. The convergence requires about 1000 function calls and it is achieved within 2 min.

Figures 3 to 10 present the minimum-time trajectories found for the different transfer configurations:

- The initial perigee local time is 0 h in Figures 3 and 4, 6 h in Figures 5 and 6, or 12 h in Figures 7 and 8.
- The initial date is the equinox in Figures 3, 5, and 7 or the solstice in Figures 4, 6, and 8.
- The thrust level is 1 N in Figures 2 to 8 and 0.1 N in Figures 9 and 10. The 0.1 N cases are computed at the equinox for local perigee times of 0 h and 12 h.

The left plot of each figure shows the trajectory projection on the equatorial plane (X, Y). The shadow region (null thrust) is represented by black bold lines on Figures 3 to 8 and by white lines on Figures 9 and 10 to be better distinguished. The shadow region rotates simultaneously with the apparent Sun motion at a 0.986°/day rate. The thrust direction is indicated by arrows during the first and the last revolution. The right plots of each figure show the respective evolutions of the apogee, the perigee, the inclination, and the cumulated eclipse duration.

Transfers starting at the equinox (Figures 3, 5, and 7) yield the longest eclipse durations, because the Sun lies in the equatorial plane, which is the final targeted plane. Conversely, transfers starting at the solstice (Figures 4, 6 and 8) yield the shortest eclipse durations because the Sun lies at a 23.45° latitude, far outside the targeted equatorial plane. In this configuration, the final GEO orbit is fully in light and the last part of the transfer does not enter the shadow region. For a solstice transfer starting with a 12 h perigee local time (Figure 8), there is even no eclipse at all since the low altitude part of the transfer occurs on the lightened side of the Earth.

With a thrust level of 1 N (Figures 3 to 8), the transfer is achieved in less than one month, so that the Sun direction moves at most of 30° during the transfer. Eclipses occur only at the transfer beginning and reduce progressively while the vehicle is gaining altitude. The eclipse duration ranges from 0 h to 44 h.

When the thrust level is decreased to 0.1 N (Figures 9 and 10), the transfer takes about eight months. Eclipses may occur both at the transfer beginning and end due to the Sun direction large change during the transfer.

Whatever the initial configuration, the transfer comprises a first part raising the apogee beyond 36,000 km and a second part bringing the apogee

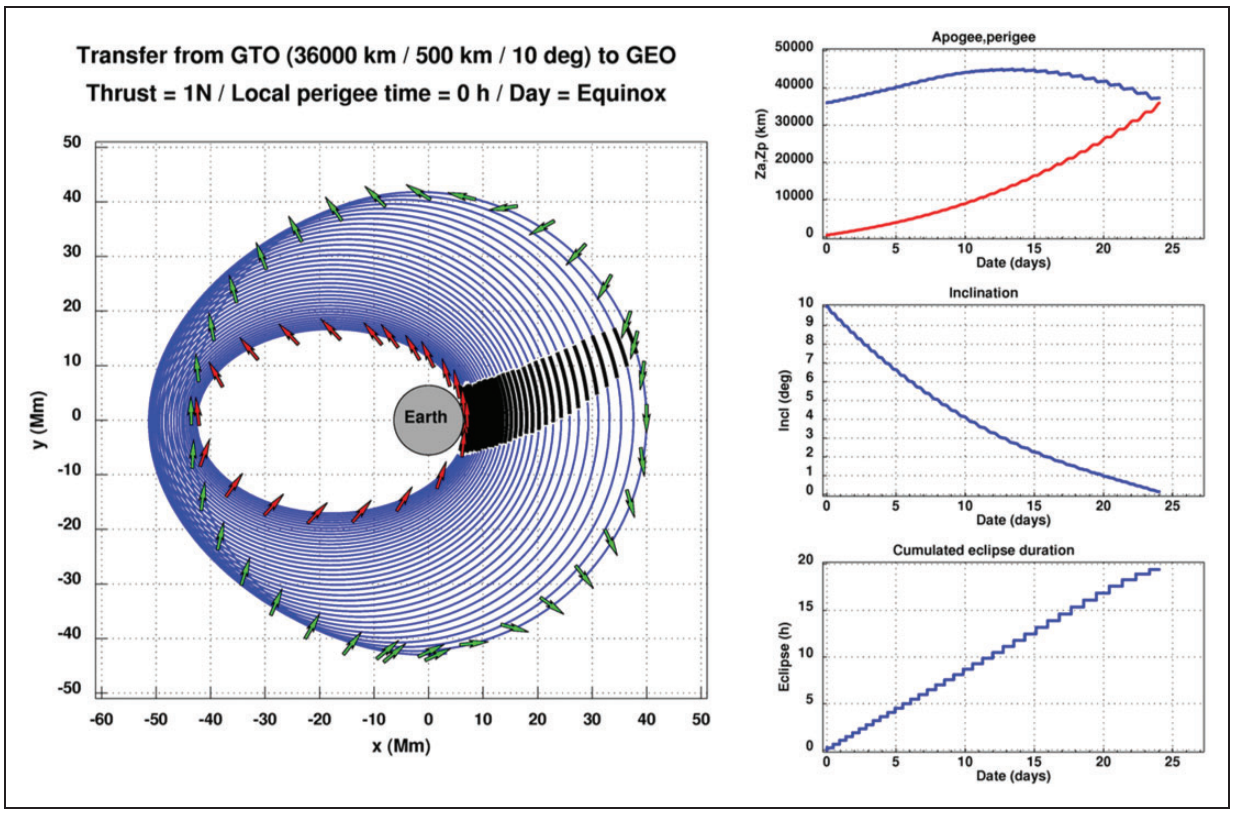

Figure 3. GTO to GEO transfer at equinox with initial local perigee time = 0 h and 1 N thrust. GTO: geostationary transfer orbit; GEO: geostationary orbit.

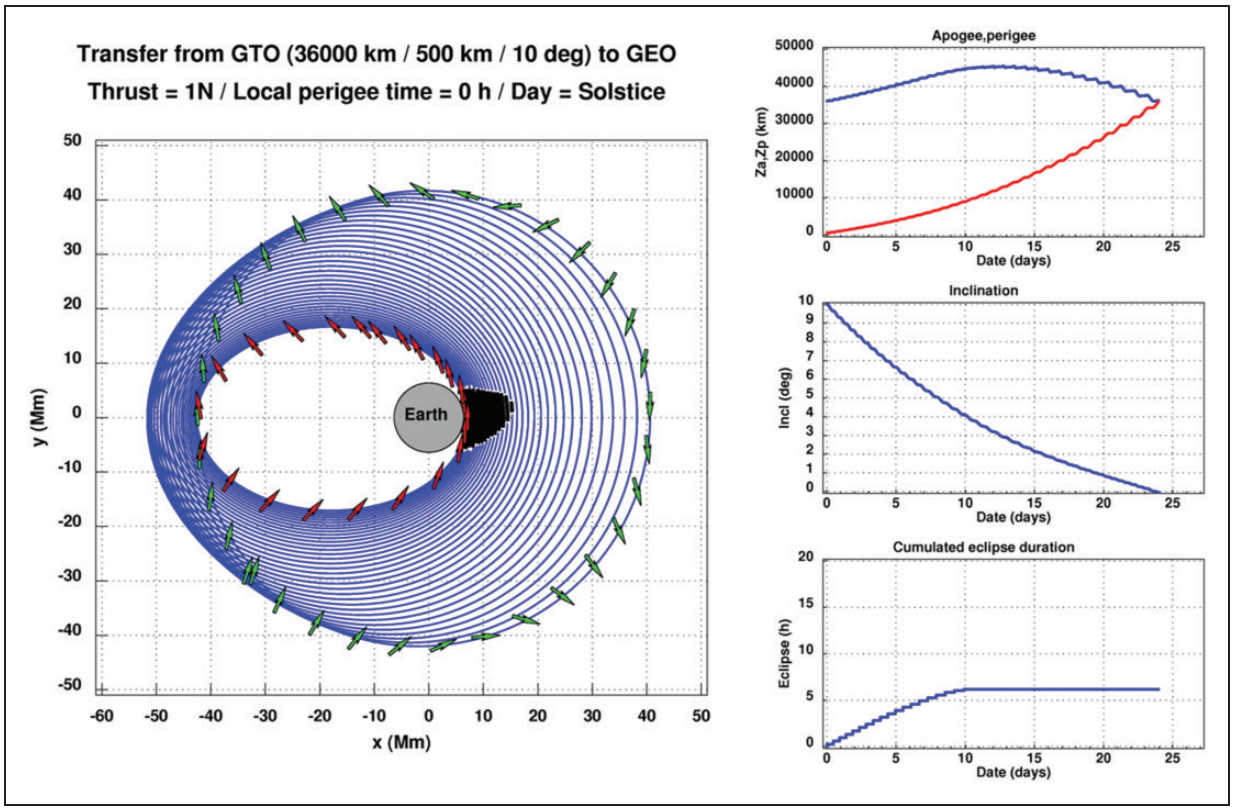

Figure 4. GTO to GEO transfer at solstice with initial local perigee time = 0 h and 1 N thrust. GTO: geostationary transfer orbit; GEO: geostationary orbit.

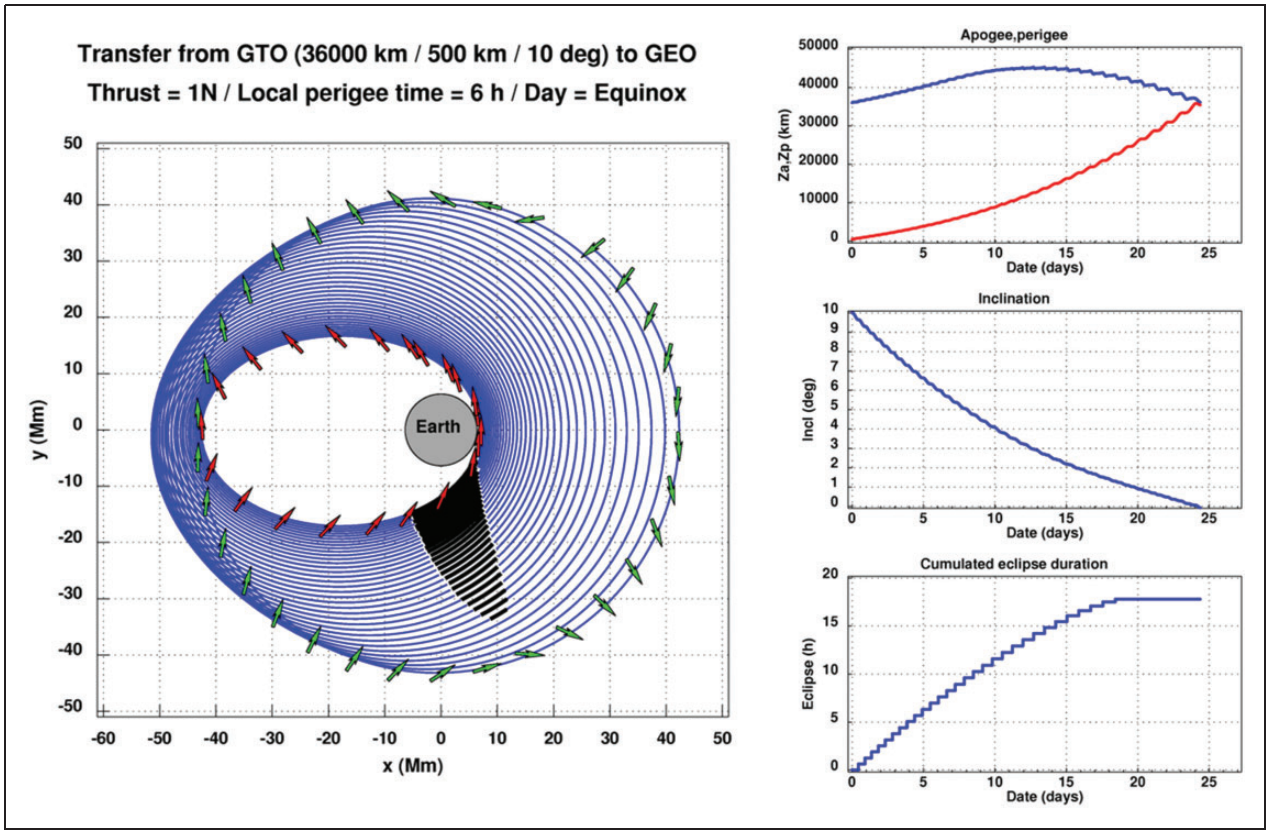

Figure 5. GTO to GEO transfer at equinox with initial local perigee time = 6 h and 1 N thrust. GTO: geostationary transfer orbit; GEO: geostationary orbit.

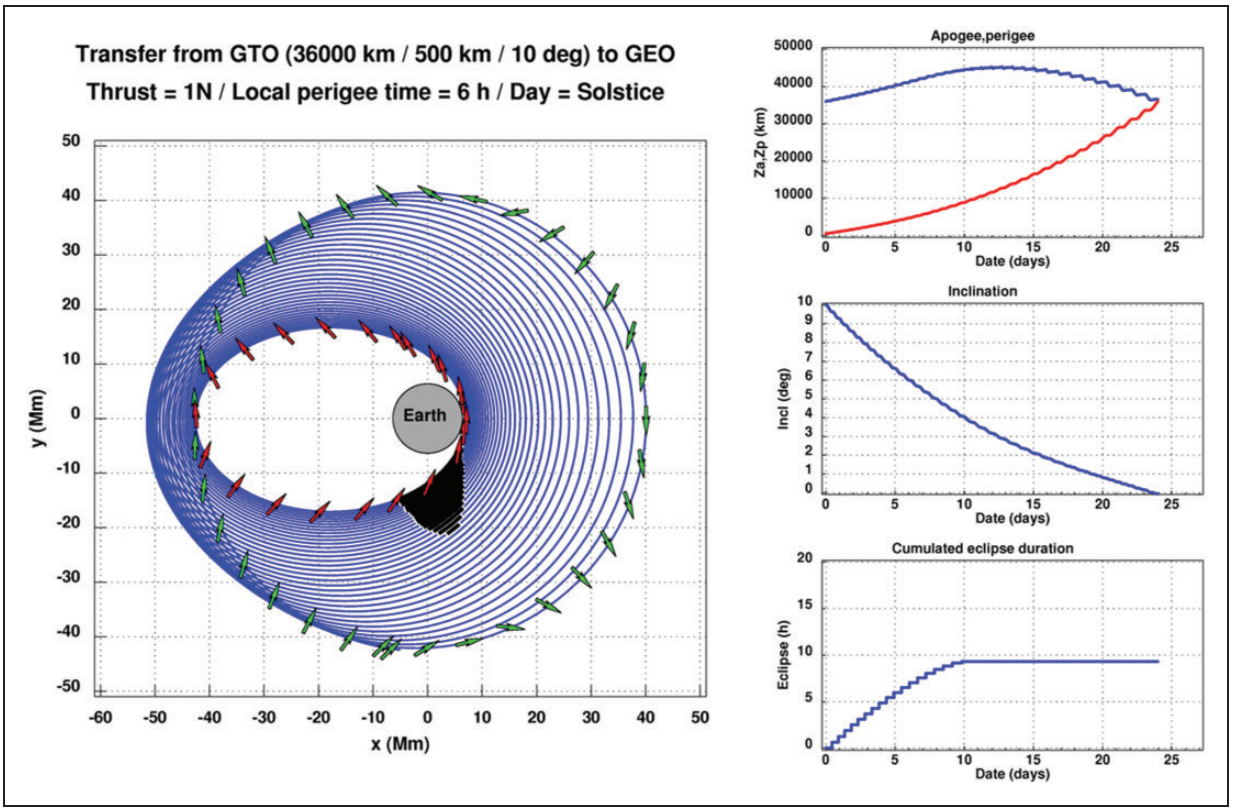

Figure 6. GTO to GEO transfer at solstice with initial local perigee time = 6 h and 1 N thrust. GTO: geostationary transfer orbit; GEO: geostationary orbit.

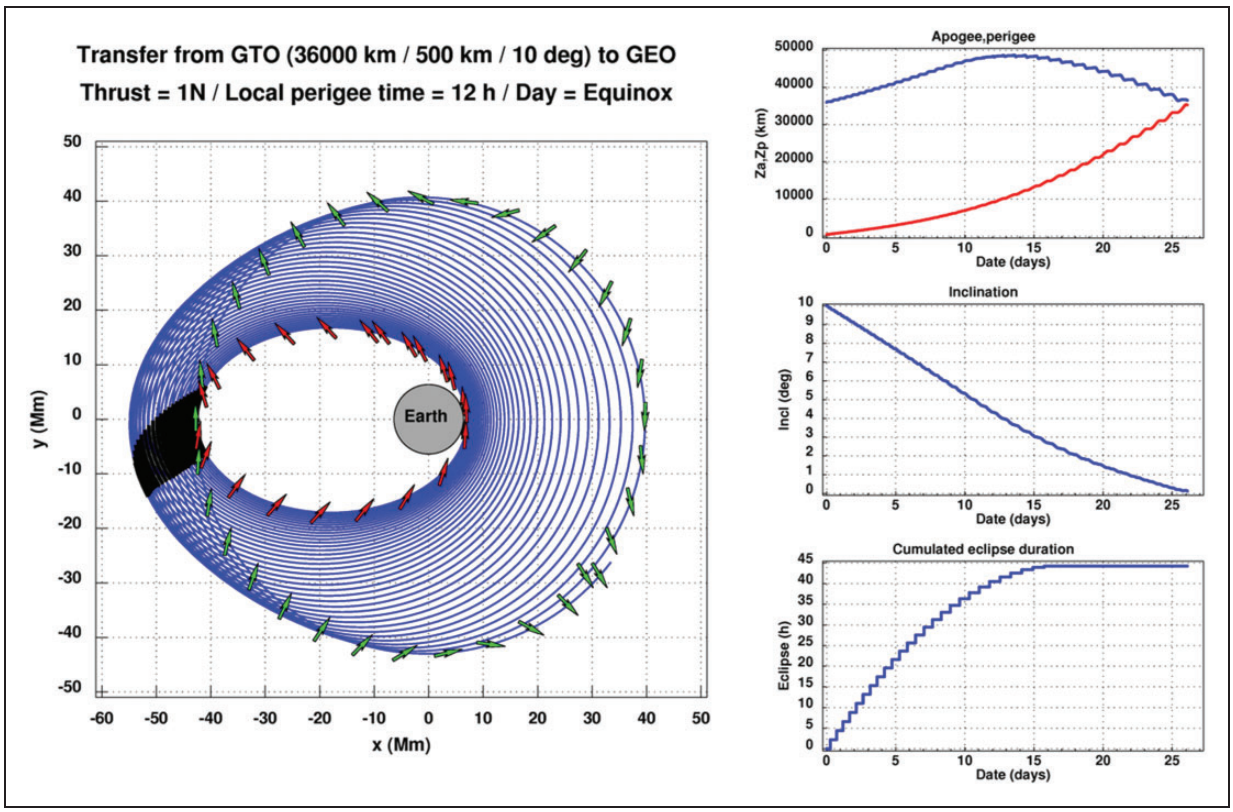

Figure 7. GTO to GEO transfer at equinox with initial local perigee time = 12 h and 1 N thrust. GTO: geostationary transfer orbit; GEO: geostationary orbit.

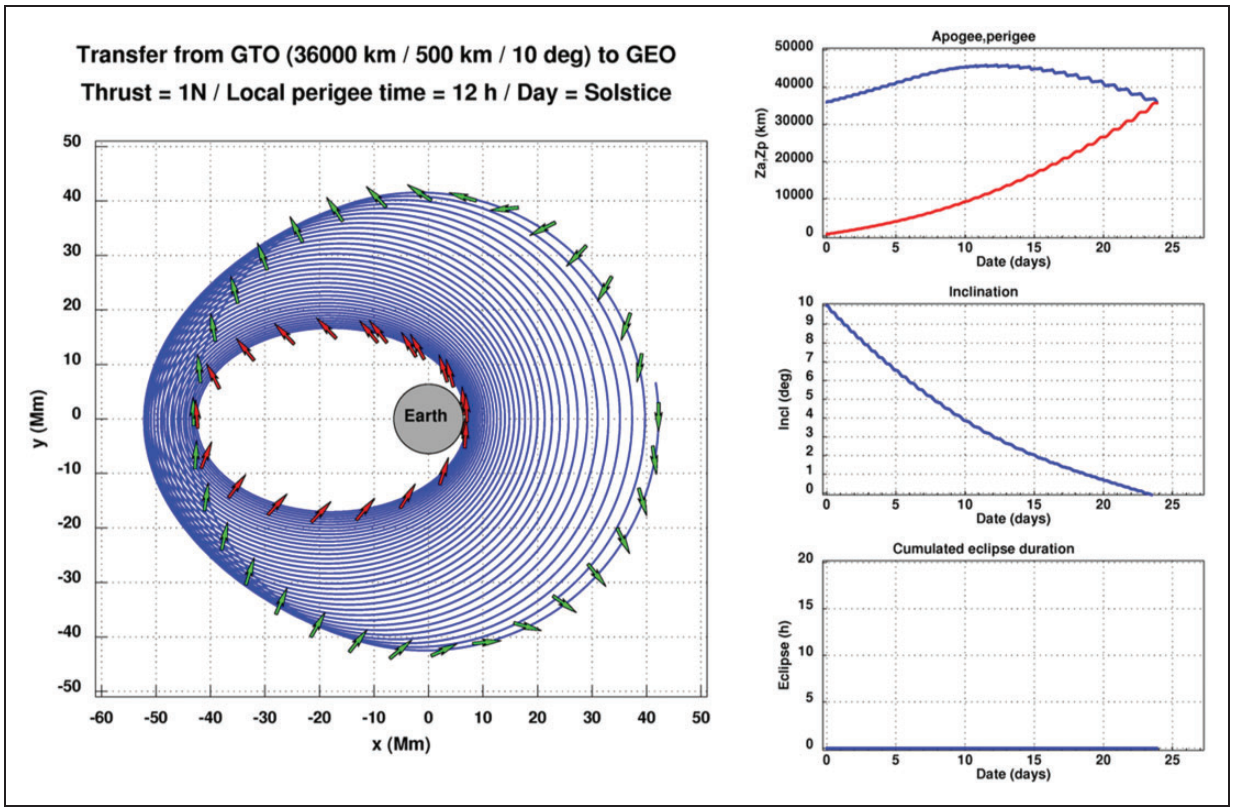

Figure 8. GTO to GEO transfer at solstice with initial local perigee time = 12 h and 1 N thrust. GTO: geostationary transfer orbit; GEO: geostationary orbit.

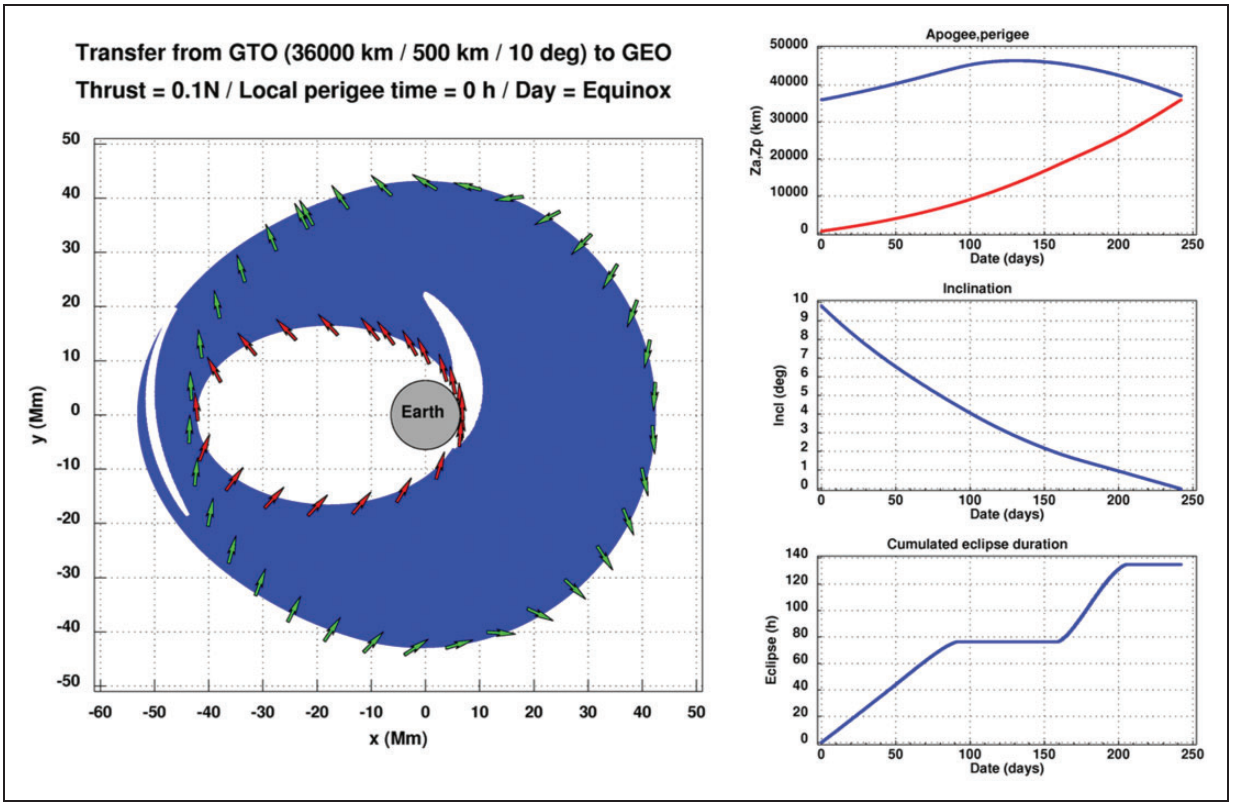

Figure 9. GTO to GEO transfer at equinox with initial local perigee time = 0 h and 0.1 N thrust. GTO: geostationary transfer orbit; GEO: geostationary orbit.

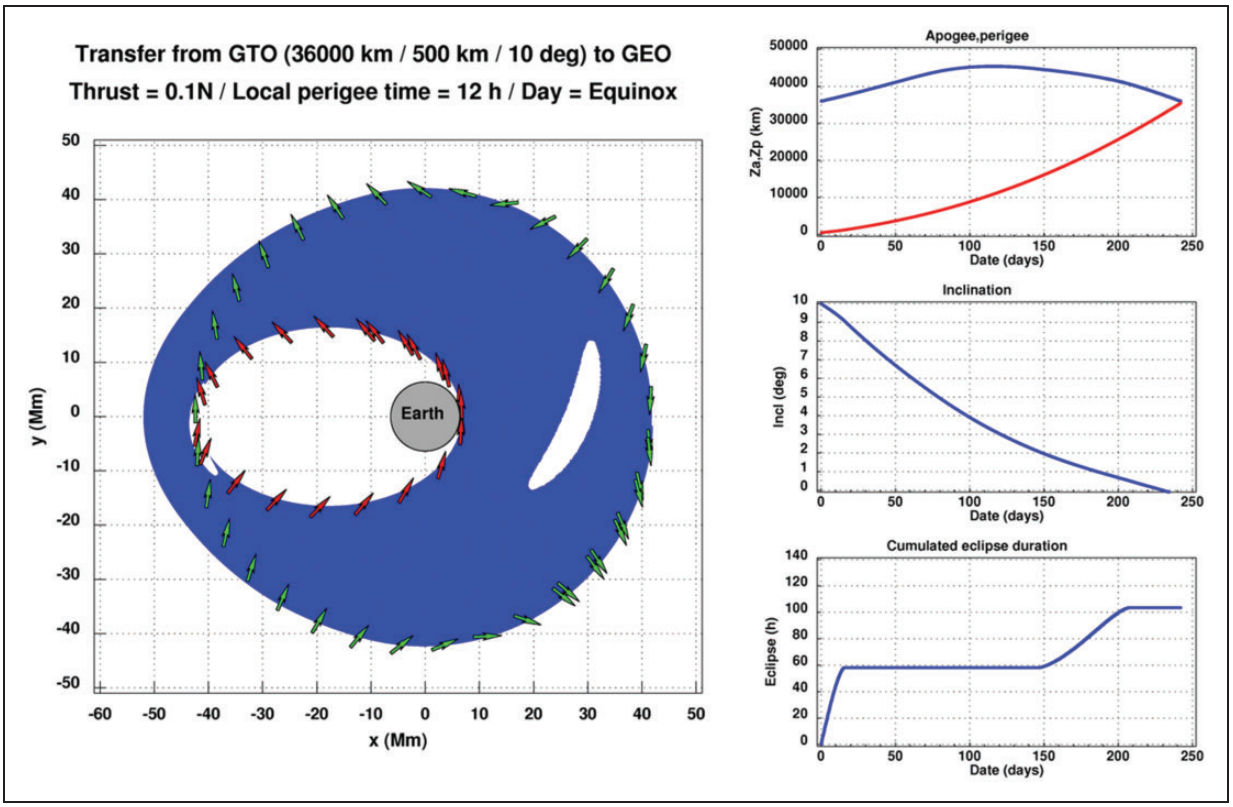

Figure 10. GTO to GEO transfer at equinox with initial local perigee time = 12 h and 0.1 N thrust. GTO: geostationary transfer orbit; GEO: geostationary orbit.

Table 1. GTO to GEO transfer for different dates and initial orbit orientations.

Thrust level (N)	1						0.1	
Transfer date	Equinox	Solstice	Equinox	Solstice	Equinox	Solstice	Equinox	Solstice
Perigee local time (h)	0 h	0 h	6 h	6 h	12 h	12 h	0 h	0 h
Final mass (kg)	863.6	860.6	861.1	861.4	857.5	859.7	861.1	860.2
Final time (day)	24.04	23.99	24.38	23.99	26.11	23.89	242.18	242.24
Velocity impulse (m/s)	2157.8	2208.2	2199.2	2195.3	2261.3	2224.0	2200.4	2214.4
Number of eclipses	34	18	29	18	26	0	219	104
Eclipse duration (h)	19.4	6.1	17.8	9.3	44.3	0.0	134.9	103.4
Angle θ_r (deg)	0.0867	0.0843	0.0823	0.0823	0.0833	0.0823	0.0856	0.0823
Angle θ_v (deg)	−4.198	−4.198	−4.198	−4.198	−4.194	−4.197	−4.188	−4.188
Angle β_r (deg)	0.000	0.000	0.000	0.000	0.000	0.000	0.000	0.000
Angle β_v (deg)	−0.0176	−0.0452	−0.0934	−0.0993	−0.0183	−0.0984	0.0635	−0.0180

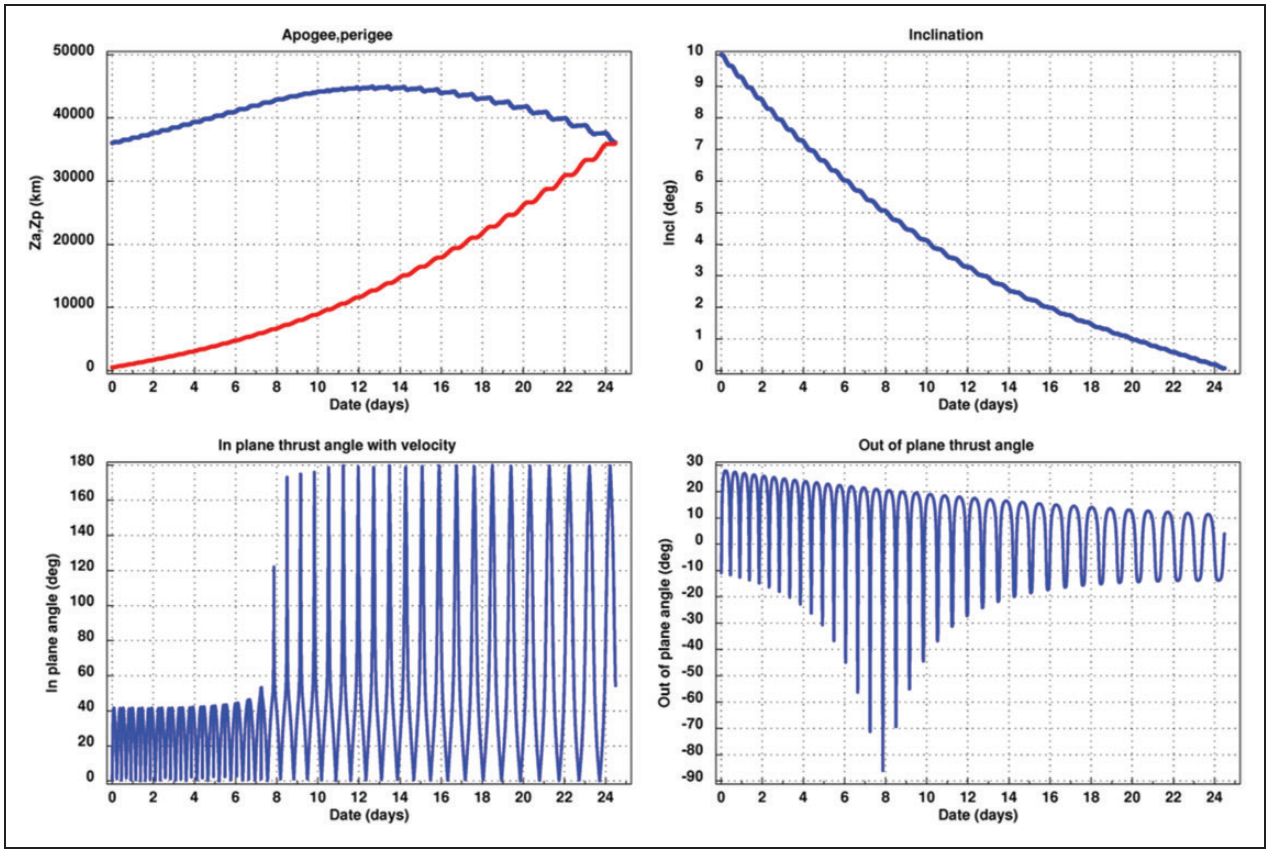

Figure 11. Thrust angle evolution (GTO-GEO at equinox with initial local perigee time = 0 h and 1 N thrust).

back to 36,000 km. The inclination change is faster during the transfer first part in order to benefit from the lower apogee velocity.

The numerical results are presented in Table 1 for the different transfer configurations.

An apogee in the Earth shadow (perigee time = 12 h) at the equinox gives the worst results since the most favorable part of the orbit is not available for thrusting. Perigee times between 0 h and 6 h yield close performances in terms of transfer duration and final mass. These two quantities are not directly linked since the eclipse location both influences the transfer duration and the thrust efficiency with respect to the orbit evolution. The four angles (θ_r, θ_v, β_r, and β_v) are close to zero as expected from the analytical costate solution derived from high-thrust transfers. It can be observed that the in-plane angle θ_v representing the initial angle of attack has nearly the same value in all cases for a given thrust level. The differences come mainly from the out-of-plane angle β_v which initiates the inclination

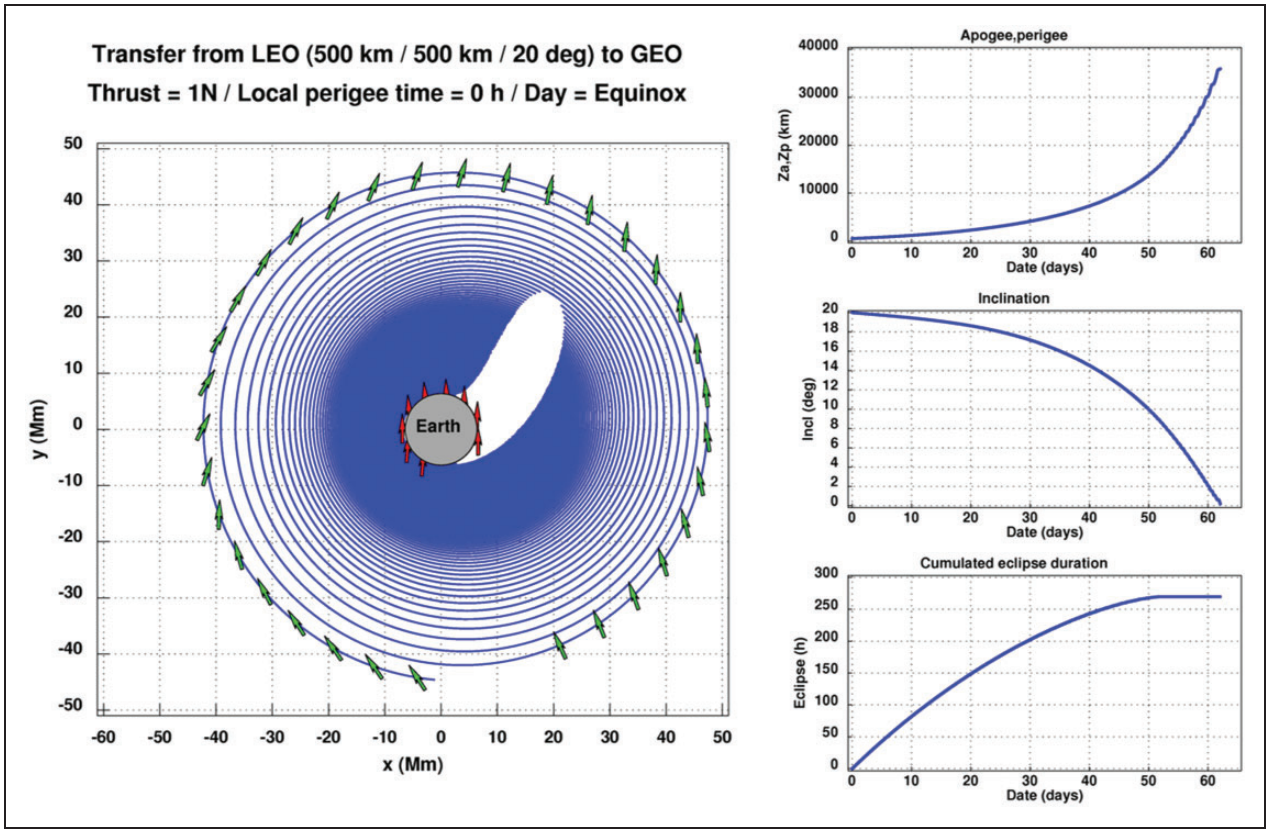

Figure 12. LEO to GEO transfer at equinox with 1 N thrust.

change. The very small differences between these solutions are in accordance with the overall sensitivity of the trajectory to the initial costate guess.

The evolution of the thrust direction is plotted on Figure 11. The in-plane angle is the angle of the velocity with the thrust projection in the local orbital plane. The out-of-plane angle is the angle of the thrust with the local orbital plane. The plots of Figure 11 correspond to the case of Figure 3 (transfer at equinox with initial local perigee time = 0 h and 1 N thrust). Two phases are observed. During the first phase (until day 8), the out-of-plane angle increases reaching 90° at day 8, while the in-plane angle remains bounded to 20°. This first phase increases the apogee altitude and performs out-of-plane thrusting near the apogee in order to benefit from a lower velocity for the inclination changes. During the second phase the out-of-plane angle reduces, while the in-plane angle oscillates between 0° at the apogee (to raise the perigee) and 180° at the perigee (to lower the apogee to the GEO altitude).

The same GTO to GEO transfer is assessed using the CNES software MIPELEC.[68,69] MIPELEC is based on an averaging method to find the minimum-time transfer without eclipse. A final mass of 860.2 kg and a final time of 23.8 days are found. These results are in accordance with the (solstice/12 h) case where no eclipse occurs.

Another comparison is made with reference[54] on a test case originating from Ferrier and Epenoy.[51] A transfer from a GTO (semi-major axis = 24,505.9 km, eccentricity = 0.725, inclination = 7.05°, right ascension of ascending node (RAAN) and perigee argument = 0°) towards the GEO is assessed considering a 0.35 N thrust, a 2000 s specific impulse and an initial mass of 2000 kg. The transfer is assessed on the first of January. A duration of 141.7 days and a consumption of 208.9 kg are found, with 197 revolutions and 148.1 h in eclipse. These results are nearly identical to those of Ferrier and Epenoy[51] and Sanchez Perez and Varga.[54]

Table 2. LEO to GEO transfer with 1 N.

Eclipse	With	Without	MIPELEC
Final mass (kg)	701.3	700.3	705.2
Final time (day)	62.1	51.0	50.2
Number of eclipses	400	0	0
Eclipse duration (h)	269.5	0	0

The solution method is finally applied to a Low Earth Orbit (LEO) to GEO transfer starting from an initial circular orbit at 500 km with an inclination of 20°, considering the same vehicle assumptions with a 1 N thrust. The trajectory is plotted on Figure 12 and the results are presented in Table 2. The comparison with MIPELEC is still correct.

Comparing the transfer durations with and without eclipse for the GTO–GEO and the LEO–GEO cases, it is observed that the rule of the thumb "difference = total eclipse duration" holds. Nevertheless,

this rule may become less accurate for transfers subject to longer eclipses, with inclinations close to 23°.

Conclusion

A solution method is proposed to assess minimum-time low-thrust transfers with eclipses, while avoiding the usual issues of indirect methods, namely the costate discontinuities at the eclipse entrance and exit, the initial costate guess sensitivity and the numerical accuracy required by the shooting method. The method proposed is based on four key elements. The first one is to apply directly the costate jumps during the trajectory simulation, when entering or exiting the shadow region. The second one is to fix the targeted final anomaly in order to discard the position and velocity transversality conditions. This allows recasting the boundary value problem as an unconstrained minimization problem. The third one is to define an analytical costate guess parameterized by four angles taking near zero values. The search space is thus significantly narrowed and it is identical whatever the application case. The fourth one is to solve the unconstrained minimization problem by a derivative-free algorithm, thus alleviating the numerical accuracy issues. Cartesian coordinates can be kept, yielding simple equations for the state, the costate and the eclipse constraint formulation. The numerical propagation uses large time steps and large tolerances, making each simulation quite fast.

The method has been applied on transfers towards the geostationary orbit for various initial dates, initial orbit orientations and engine thrust levels. In all cases, a quasi-optimal solution is found from scratch in a few minutes at most without requiring specific users' guesses or tunings from one case to another.

Declaration of Conflicting Interests

The author(s) declared no potential conflicts of interest with respect to the research, authorship, and/or publication of this article.

Funding

The author(s) received no financial support for the research, authorship, and/or publication of this article.

ORCID iD

Max Cerf http://orcid.org/0000-0002-5506-2044

References

1. Betts JT. Survey of numerical methods for trajectory optimization. *J Guid Control Dyn* 1998; 21: 193–207.
2. Rao A. A survey of numerical methods for optimal control. *Adv Astronaut Sci* 2009; 135: 497–528.
3. Kim M. Continuous low-thrust trajectory optimisation: techniques and applications. PhD Thesis, Virginia Polytechnic Institute and State University, USA, 2005.
4. Hargraves CR and Paris SW. Direct trajectory optimization using nonlinear programming and collocation. *J Guid Control Dyn* 1987; 10: 338–342.
5. Enright PJ and Conway BA. Discrete approximations to optimal trajectories using direct transcription and nonlinear programming. *J Guid Control Dyn* 1992; 15: 994–1002.
6. Ross IM and Fahroo F. Pseudospectral knotting methods for solving optimal control problems. *J Guid Control Dyn* 2004; 27: 397–405.
7. Paris SW, Riehl JP and Sjauw WK. Enhanced procedures for direct trajectory optimization using nonlinear programming and implicit integration. In: *Proceedings of the AIAA/AAS astrodynamics specialist conference and exhibit*, August 2006, pp.21–24.
8. Dileep MV, Nair VG, Prahalad KR, et al. Trajectory optimization of launch vehicles using steepest descent method – a novel approach ascent optimization for a heavy space launcher. *Int J Eng Res Appl* 2014; 4: 116–121.
9. Betts JT. *Practical methods for optimal control and estimation using nonlinear programming*. Philadelphia: Siam, 2010.
10. Topputo F and Zhang C. Survey of direct transcription for low-thrust space trajectory optimization with applications. *Abstr Appl Anal* 2014; 2014: 851720.
11. Betts JT. Very low thrust trajectory optimization using a direct SQP method. *J Comput Appl Math* 2000; 120: 27–40.
12. Betts JT. Optimal low thrust orbit transfer with eclipsing. *OCAM* 2015; 36: 218–240.
13. Lawden DF. Optimal transfer between coplanar elliptical orbits. *J Guid Control Dyn* 1991; 15: 788–791.
14. Broucke RA and Prado AFBA. Optimal N-impulse transfer between coplanar orbits. In: *AAS/AIAA astrodynamics specialist conference*, Victoria, Canada, 1994.
15. Yam CH, Izzo D and Biscani F. *Towards a high fidelity direct transcription method for optimisation of low-thrust trajectories*. Noordwijk: ESTEC, 2011.
16. Landau DF and Longuski JM. Trajectories for human missions to Mars, Part 2: low thrust transfers. *J Spacecr Rockets* 2006; 43: 1043–1047.
17. Pontryagin L, Boltyanskii V, Gramkrelidze R, et al. *The mathematical theory of optimal processes*. New York: Wiley Interscience, 1962.
18. Trélat E. *Contrôle optimal – Théorie et applications*. Paris: Vuibert, 2005.
19. Conway BA. *Spacecraft trajectory optimization*. New York: Cambridge University Press, 2010.
20. Lawden DF. *Optimal trajectories for space navigation*. London: Butterworths Publishing Corporation, 1963.
21. Leitmann G. *Optimization techniques with applications to aerospace system*. New York: Academic Press, 1962.
22. Marec JP. *Optimal space trajectories*. Amsterdam: Elsevier, 1979.
23. Bonnard B, Caillau J-B and Trélat E. Geometric optimal control of elliptic Keplerian orbits. *Discrete Cont Dyn Syst* 2005; 5: 929–956.
24. Caillau J-B and Noailles J. Coplanar control of a satellite around the Earth, ESAIM Cont. *Optim Calc Var* 2001; 6: 239–258.
25. Martinon P and Gergaud J. Using switching detection and variational equations for the shooting method. *Optim Control Appl Methods* 2007; 28: 95–116.

26. Bonnans F, Martinon P and Trélat E. Singular arcs in the generalized Goddard's problem. *J Optim Theor Appl* 2008; 139: 439–461.
27. Ponssard P, Graichen K, Petit N, et al. Ascent optimization for a heavy space launcher. In: *Proceedings of the European control conference 2009*, Budapest, Hungary, 23–26 August 2009.
28. Augros P, Delage R and Perrot L. *Computation of optimal coplanar orbit transfers*. Reston: AIAA, 1999.
29. Naidu DS, Hibey JL and Charalambous C. Fuel-optimal trajectories for aeroassisted coplanar orbital transfer problem. *IEEE Trans Aerosp Electron Syst* 1990; 26: 374–381.
30. Gergaud J and Haberkorn T. Orbital transfer: some links between the low-thrust and the impulse cases. *Acta Astronaut* 2007; 60: 649–657.
31. Lee D and Bang H. Efficient initial costates estimation for optimal spiral orbit transfer trajectories design. *J Guid Control Dyn* 2009; 32: 1943–1947.
32. Pifko SL, Zorn AH and West M. Geometric interpretation of adjoint equations in optimal low thrust space flight. In: *AIAA/AAS astrodynamics specialist conference and exhibit*, Honolulu, Hawaii, 18–21 August 2008.
33. Oberle HJ and Taubert K. Existence and multiple solutions of the minimum-fuel orbit transfer problem. *J Optim Theory Appl* 1997; 95: 243–262.
34. Graham KF and Rao AV. Minimum-time trajectory optimization of low thrust earth-orbit transfers with eclipsing. In: *AAS/AIAA space flight mechanics meeting*, Williamsburg, Virginia, 11–15 January 2015.
35. Jiang F, Baoyin H and Li J. Practical techniques for low-thrust trajectory optimization with homotopic approach. *J Guid Control Dyn* 2012; 35: 245–258.
36. Gergaud J, Haberkorn T and Martinon P. Low thrust minimum fuel orbital transfer: an homotopic approach. *J Guid Control Dyn* 2004; 27: 1046–1060.
37. Haberkorn T and Trélat E. Convergence results for smooth regularizations of hybrid nonlinear optimal control problems. *SIAM J Control Optim* 2011; 49: 1498–1522.
38. Thorne JD and Hall CD. Minimum-time continuous thrust orbit transfers. *J Astronaut Sci* 1997; 47: 411–432.
39. Dargent T and Martinot V. An integrated tool for low thrust optimal control orbit transfers in interplanetary trajectories. In: *Proceedings of the 18th international symposium on space flight dynamics* (ESA SP-548), Munich, Germany, 11–15 October 2004.
40. Pontani M and Conway BA. Particle swarm optimization applied to space trajectories. *J Guid Control Dyn* 2010; 33: 1429–1441.
41. Steffens MJ. *A combined global and local methodology for launch vehicle trajectory design-space exploration and optimization*. Thesis, Georgia Institute of Technology, USA, April 2014.
42. Zuiani F. *Multi-objective optimization of low-thrust trajectories*. PhD Thesis, University of Glasgow, UK, 2015.
43. Bérend N, Bonnans F, Haddou M, et al. An interior-point approach to trajectory optimization. *J Guid Control Dyn* 2007; 30: 1228–1238.
44. Bourgeois E, Bokanowski O, Zidani H, et al. Optimization of the launcher ascent trajectory leading to the global optimum without any initialization: the breakthrough of the HJB approach. In: *6th European conference for aeronautics and space sciences* (EUCASS), Kraków, Poland, 29 June 2015–2 July 2015.
45. Kechichian JA. Low-thrust eccentricity-constrained orbit raising. *J Spacecr Rockets* 1998; 35: 327–335.
46. Kechichian JA. Orbit raising with low-thrust tangential acceleration in presence of earth shadow. *J Spacecr Rockets* 1998; 35: 516–525.
47. Kechichian JA. Low-thrust inclination control in presence of earth shadow. *J Spacecr Rockets* 1998; 35: 526–532.
48. Kluever CA and Oleson SR. Direct approach for computing near-optimal low-thrust earth-orbit transfers. *J Spacecr Rockets* 1998; 35: 509–515.
49. Gao Y. Near-optimal very low-thrust earth-orbit transfers and guidance schemes. *J Guid Control Dyn* 2007; 30: 529–539.
50. Yang G. Direct optimization of low-thrust many-revolution earth-orbit transfers. *Chin J Aeronaut* 2009; 22: 426–433.
51. Ferrier C and Epenoy R. Optimal control for engines with electro-ionic propulsion under constraint of eclipse. *Acta Astronaut* 2001; 48: 181–192.
52. Petropoulos AE. Low-thrust orbit transfers using candidate Lyapunov functions with a mechanism for coasting. In: *AIAA/AAS astrodynamics specialist conference*, AIAA Paper 2004-5089, Providence, Rhode Island, 16–19 August 2004.
53. Petropoulos AE. Refinements to the q-law for low thrust orbit transfers. In: *AAS space flight mechanics meeting*, AAS Paper 05-162, Cooper Mountain, Colorado, 23–27 January 2005.
54. Sanchez Perez JM and Varga GI. Many-revolution low thrust orbit transfer computation using equinoctial q-law including J2 and eclipse effects. In: *AIAA/AAS astrodynamics specialist conference*, AIAA/AAS Paper 15-590, Vail, CO, 2015.
55. Bryson AE and Ho YC. *Applied optimal control*. Washington, DC: Hemisphere Publishing Corporation, 1975.
56. Hull DG. *Optimal control theory for applications*. New York: Springer, 2003.
57. Vallado DA. *Fundamentals of astrodynamics and applications*. 3rd ed. El Segundo: Microcosm Press, 2007.
58. Bombrun A and Pomet J-B. Asymptotic behavior of time optimal orbital transfer for low thrust 2-body control system. *Discrete Contin Dyn Sys* 2007; Supplement 2007: 122–129.
59. Thorne JD. Minimum-time constant-thrust orbit transfers with noncircular boundary conditions. In: *Proceedings of the advanced Maui optical and space surveillance technologies conference*, Wailea, Maui, Hawaii, 10–13 September 2013.
60. Cerf M. Optimal thrust level for orbit insertion. *Acta Astronautica* 2017; 136: 55–63.
61. Vugrin KE. *On the effect of numerical noise in simulation-based optimization*. Thesis, Faculty of the Virginia Polytechnic Institute and State University, USA, March 2003.
62. Di Pillo G, Lucidi S and Rinaldi F. A derivative-free algorithm for constrained global optimization based on exact penalty functions. *J Optim Theor Appl* 2015; 164: 862–882.

63. Parsopoulos KE and Vrahatis MN. Particle swarm optimization method for constrained optimization problems. In: *Proceedings of the Euro-International symposium on computational intelligence: Frontiers in artificial intelligence and applications*. Amsterdam: IOS Press, 2002, pp. 214–220.
64. Paluszek MA and Thomas SJ. Trajectory optimization using global methods. In: *29th International electric propulsion conference*, IEPC05-173, Princeton University, Princeton, NJ, USA, 31 October 2005–4 November 2005.
65. Perttunen CD, Jones DR and Stuckman BE. Lipschitzian optimization without the Lipschitz constant. *J Optim Theor Appl* 1993; 79: 157–181.
66. Gablonsky JM. Direct version 2.0 userguide. Technical Report, CRSC-TR01-08, Center for Research in Scientific Computation, North Carolina State University, April 2001.
67. Liuzzi G, Lucidi S and Piccialli V. *Exploiting derivative-free local searches in direct-type algorithms for global optimization*. Rome: Istituto di Analisi dei Sistemi ed Informatica "A. Ruberti," 2014.
68. Geffroy S. *Généralisation des techniques de moyennation en contrôle optimal – application aux problèmes de transfert et rendez-vous orbitaux à poussée faible*. Thèse de doctorat, Institut National Polytechnique de Toulouse, France, 1997.
69. Geffroy S and Epenoy R. Optimal low-thrust transfers with constraints – generalization of averaging techniques. *Acta Astronaut* 1997; 41: 133–149.